# Unoccupied Band Structure of $NbSe_2$ by Very-Low-Energy Electron Diffraction: Experiment and Theory

E. E. Krasovskii and W. Schattke
*Institut für Theoretische Physik, Christian-Albrechts-Universität, Leibnizstrasse 15, D-24098 Kiel, Germany*

V. N. Strocov† and R. Claessen
*Experimentalphysik II, Universität Augsburg, D-86135 Augsburg, Germany*

arXiv:cond-mat/0207607 v1 25 Jul 2002

A combined experimental and theoretical study of very-low-energy electron diffraction at the (0001) surface of 2H-$NbSe_2$ is presented. Electron transmission spectra have been measured for energies up to 50 eV above the Fermi level with $\mathbf{k}^{||}$ varying along the ΓK line of the Brillouin zone. *Ab initio* calculations of the spectra have been performed with the extended linear augmented plane wave $\mathbf{k}\cdot\mathbf{p}$ method. The experimental spectra are interpreted in terms of three-dimensional $\mathbf{k}^{||}$-resolved one-electron band structure. Special attention is paid to the quasi-particle lifetimes: by comparing the broadening of the spectral structures in the experimental and calculated spectra the energy dependence of the optical potential $-iV_{\rm i}$ is determined. A sharp increase of $V_{\rm i}$ at 20 eV is detected, which is associated with a plasmon peak in the $\mathrm{Im}[-1/\varepsilon]$ function. Furthermore, the electron energy loss spectrum and the reflectivity of $NbSe_2$ are calculated *ab initio* and compared with optical experiments. The obtained information on the dispersions and lifetimes of the unoccupied states is important for photoemission studies of the 3D band structure of the valence band.

## I. INTRODUCTION

Very-Low-Energy Electron Diffraction (VLEED) spectroscopy with incident electron energies below $\sim 40$ eV has recently been established as the experimental method giving a direct access to dispersions $E(\mathbf{k})$ and lifetimes of quasi-particle states above the vacuum level (see Refs. 1–4 and references therein). The VLEED spectral structures reveal the critical points in the surface-perpendicular dispersions $E(k^{\perp})$ of the states that couple to the incident electron beam to form the LEED state. The fundamental advantage of the VLEED spectroscopy over the conventional unoccupied band structure methods, such as inverse photoemission or X-ray absorption spectroscopy, is that it does not involve initial states and in particular cases, for example at high-symmetry lines parallel to the surface, is capable of restoring 3D Bloch vectors $\mathbf{k}$.

Within a quasi-particle picture[5,6] the time-reversed LEED states serve as the final states of the one-step photoemission theory. Independent information on their dispersions and lifetimes provided by the VLEED experiment can be used in the photoemission experiment to resolve the valence band structure in the surface-perpendicular direction,[2,3] which is often blurred by the complicated non-free-electron-like dispersion and strong self-energy effects in the final states. In particular, the broadening of the VLEED spectral structures provides information on the lifetimes of the final state quasi-particles, which can be used to estimate the $k^{\perp}$ broadening of the Bloch constituents of the LEED state and thereby to judge on the intrinsic uncertainty of the band mapping.

Within a simplified one-particle approach, the LEED problem reduces to solving the Schrödinger equation for a semi-infinite crystal given the energy $E$ and the initial conditions of the incident electron, i.e., the asymptotics of the wave function in the vacuum. In the plane parallel to the crystal surface the LEED wave function obeys the Bloch theorem and is characterized by the 2D Bloch vector $\mathbf{k}^{||}$. In the vacuum, far from the crystal surface, it is a superposition of plane waves: the plane wave propagating towards the crystal defines incident current, and the total current carried by the LEED state is the transmitted current. The ratio of the two currents is the transmission coefficient $T(E)$. In the bulk the LEED wave function is a superposition of propagating (real $k^{\perp}$) and evanescent (complex $k^{\perp}$) Bloch waves.

This approach neglects inelastic scattering, so that in the case of a non-zero transmission the LEED state necessarily includes a propagating Bloch wave. In what follows the propagating constituents are referred to as conducting states. Gross features of the $T(E)$ spectrum depend upon the band structure of the bulk crystal: the energies at which the band ceases transmitting the current (e.g. when the group velocity vanishes) and other critical points are reflected in experimental spectra. For example, $T(E)$ drops abruptly to zero when an energy gap in the $\mathbf{k}^{||}$ projected band structure is encountered. However, owing to inelastic processes, one never observes zero transmission in the experiment, and instead of a sharp drop predicted by the simple theory one observes a rather smooth decrease of the transmission as a sign of the critical point.

In 1937 Slater[7] showed that the broadening of the spectral structures and the absence of energy gaps can be reproduced by adding an imaginary term, the optical potential $-iV_{\rm i}$, to the potential in the crystal half-space.

Slater's idea is to associate the effect of the optical potential with a spatial damping of the wave functions rather than with a decay in time. Then the Bloch vector acquires an imaginary part of the order of $V_{\rm i}/\hbar v^{\perp}$ ($v^{\perp}$ is the group velocity), or, in terms of the mean free path $d = 1/{\rm Im}k$, it is $V_{\rm i} = \hbar v^{\perp}/d$. The optical potential is, thus, understood as the inverse lifetime of the quasiparticle. Alternatively, one can think of an electron with a lifetime $\tau = \hbar/V_{\rm i}$ and mean free path $1/{\rm Im}k$ that moves in a real non-absorbing potential.[1] In the present work we make an attempt to extract quantitative information on the energy dependence of $V_{\rm i}$ from the measured $T(E)$ spectra by comparing the broadening of experimental and calculated spectral structures.

The unoccupied band structures of layered quasi-2D materials, such as graphite[8] or transition metal dichalcogenides,[2,9,10] are particularly interesting: owing to the interlayer potential barrier, a nearly-free-electron model fails to provide even a qualitative picture of the unoccupied states. The necessity to describe such states within an all-electron approach for the crystal potential of general shape and to understand their relation to the diffraction process has been a driving force of the development of the Bloch-wave-based *ab initio* methodology.[11–14] In this work, we use the extended linear augmented plane wave (ELAPW) $\mathbf{k}\cdot\mathbf{p}$ method,[15] whose distinctive feature is that it reduces the inverse band structure problem – finding $k^{\perp}$ given $\mathbf{k}^{||}$ and $E$ – to a matrix eigenvalue problem.

Of the layered materials, the band structure of 2H-$NbSe_2$ deserves special attention. Its Fermi surface comprises two cylindrical sheets and a tiny 3D electron pocket near the Γ point,[16,17] all having different superconducting properties.[18] Mapping of this pocket in the photoemission experiment is complicated by that its extension in $k^{\perp}$ is comparable with the final state $k^{\perp}$ broadening,[19,20] and it relies critically on the knowledge of not only the final state dispersion but also lifetime.

In this paper, we present experimental electron transmission spectra of $NbSe_2$ and compare them to our *ab initio* calculations. The experimental technique is described in Sec. II. A brief account of our self-consistent band structure calculation is given in Sec. III and the computational method for LEED states is presented in Sec. IV. The experimentally observed broadening of spectral structures is reproduced by including an imaginary part of the potential $V_{\rm i}$ into the Hamiltonian. In Sec. V we describe a procedure to obtain quantitative information on the quasi-particle lifetimes from the analysis of the shape of the experimental spectra. The observed energy dependence of the optical potential is interpreted in terms of electron energy loss function. In Sec. VI we present the unoccupied band structure of $NbSe_2$ in the ΓK direction and discuss possible limitations of the common description of the inelastic scattering by an optical potential. Optical properties are discussed in Sec. VII.

## II. EXPERIMENTAL

Essential details of our VLEED experimental technique are given elsewhere.[3,21] Briefly, we used a standard 4-grid LEED optics operating in the retarding field mode. In this mode the electrons are accelerated in the gun to the energies required to form a well-focussed beam (normally from 100 to 300 eV) and then decelerated in a retarding field between the gun and the sample. This mode allows us to achieve the lowest primary energies without any significant degradation in focussing. However, angle dependent measurements are complicated by that the retarding field distorts the off-normal electron trajectories. To determine $\mathbf{K}^{||}$, we parameterized its dependence on energy $E$ and the sample rotation angle $\alpha$ by a biquadratic function $K^{||}(E,\alpha) = \sum_{l,m=0}^{2} A_{lm}E^{l}\alpha^{m}$ with the coefficients $A_{lm}$ fixed by fitting to the experimental points with well-defined $K^{||}$, namely to the angle dependent target current onsets, in which $K^{||}=\sqrt{2m\,(E-e\phi)}\,/\hbar$, and to the characteristic diffraction patterns when a diffracted beam hits the electron gun exit, in which $\mathbf{K}^{||}$ equals half the surface reciprocal lattice vector $\mathbf{G}^{||}/2$ (see Ref. 21 for details).

The present experiment was carried out on an improved setup: Screening from the stray magnetic fields using $\mu$-metal shielding reduced the displacement of the electron beam on the sample to less than 0.5 mm over the whole energy range. The position of the diffracted beams in the area obscured by the electron gun was controlled using a miniature fluorescent screen covered by ZnO:Zn low-energy phosphor,[22] which was mounted at the gun exit. Careful adjustment of the incidence angles was achieved using a custom made sample holder with 3 angular degrees of freedom. This is particularly important for the flaky crystals of layered materials, whose surface after gluing to the sample holder can appear a few degrees off. The tilt angle adjustment was coupled to the linear shaft motion of our standard manipulator, and the azimuthal angle was adjusted using an additional fork mounted on a rotary wobble stick. This design guaranteed the incidence angle adjustment accuracy better than 0.25° in all angular degrees of freedom. A symmetric design of the sample holder prevented distortion of the electron trajectories in the retarding field. The energy spread of the primary beam was ∼0.25 eV HWHM. The size of the beam spot on the sample can be estimated as less than 0.5 mm through the whole experimental energy range.

As a practical matter, it should be noted that during the angle-dependent measurements the electron spot can slightly displace along the surface due to the retarding field and mechanical drifts in the manipulator. This displacement can be a problem for the layered materials, whose crystals closer to the periphery typically incorporate minor misoriented crystallites. The sample position should therefore be optimized to avoid the misoriented

crystallites in the whole experimental energy and angle range. This can be controlled most easily by inspecting the diffraction patterns on the screen. In this respect the VLEED experimental setups based on the LEED electron optics have an advantage over the inverse photoemission based ones.

The experimental system provided two measurement modes: 1) measurements of the elastic reflectivity into individual diffracted beams, often referred to as the VLEED technique, using the LEED screen and a CCD camera, and 2) measurements in the target current, commonly referred to as the Target (or total, absorbed) Current Spectroscopy (TCS) technique – see, e.g., Ref. 23. The VLEED mode gives most detailed information about the diffraction process, but its principal limitation is that the reflected intensities in the area obscured by the electron gun can not be measured (e.g. the specular beam near the normal incidence). The TCS mode is free of this problem and also benefits from greater experimental simplicity, but its limitation is that the target current $I(E)$ gives the *total* reflectivity which includes the elastic reflectivity $R(E)$ integrated over all diffracted beams and, in addition, the inelastic reflectivity $R_{\rm inel}(E)$ corresponding to the secondary electrons that leave the crystal. The inelastic contribution gives, however, only a rather featureless background, so the structures in the $I(E)$ curves reflect essentially the elastic electron transmission $T(E) = 1 - R(E)$, which contain the band structure information (the derivatives $dI/dE$ and $dT/dE$ are practically equivalent).

The term VLEED will further be used in reference to the dominant physical mechanism forming the spectral structures in the individual beams as well as in the total reflectivity, rather than to the experimental technique. In this context we will refer to the target current spectra also as the VLEED spectra.

Atomically clean (0001) surfaces of $NbSe_2$ were obtained by standard cleavage in the vacuum chamber at a base pressure of $7 \times 10^{-10}$ mbar. Compared to other layered materials, the lifetime of the $NbSe_2$ surface is small: in a day after cleavage the spectral contrast significantly decreased and the background in the LEED patterns increased, indicating strong surface contamination.

## III. BAND STRUCTURE

The calculations are performed with the ELAPW $\mathbf{k}\cdot\mathbf{p}$ method.[15,24,25] The self-consistent potential was constructed within the local density approximation (LDA) of the density functional theory with the full-potential augmented Fourier components technique described in Ref. 24. The basis set included 487 energy independent APWs (energy cutoff 10.2 Ry), and the extension of the radial basis set contributed another 200 basis functions. The extension was introduced following the prescriptions of Ref. 25. The Brillouin zone (BZ) integrations were performed by the tetrahedron method with a mesh of 550 $\mathbf{k}$ points that divides the irreducible BZ into 2187 tetrahedra.

All the occupied states down to the Nb 4*p* semi-core band (at -31 eV) are treated as valence states. The density-of-states (DOS) function is in good agreement with the FLAPW calculation of Corcoran *et al.*[16] and with X-ray photoemission measurements of Wertheim *et al.*[26] The five peaks due to the strong Se 4*p* – Nb 4*d* hybridization have distinct counterparts in the experimental spectrum, see Fig. 1. The peak in the unoccupied DOS at 2.7 eV arises from localized states of almost pure Nb *d* character. Thus, one can expect strong dipole-allowed transitions from the Nb 4*p* band to produce an absorption peak at $\hbar\omega \sim 34$ eV (see Sec. VII). We do not observe any localized states above $E - E_F = 5$ eV; the complicated fine structure of the DOS curve for higher energies reflects a non-free-electron-like behavior of the unoccupied states.

## IV. CALCULATED VLEED SPECTRA

Our calculations are based on the Bloch waves approach to the LEED problem,[27] in which the crystal is treated as a semi-infinite system and the LEED wave function in the crystal half-space is sought as a linear combination of propagating and evanescent solutions of the Schrödinger equation for a bulk crystal potential. Our implementation of the theory in the case of a singular all-electron crystal potential has been described elsewhere.[15] Now we briefly sketch the computational procedure.

### A. Inverse Band Structure Problem

In the ELAPW-$\mathbf{k}\cdot\mathbf{p}$ method the complex band structure can be obtained by an analytical continuation of the Schrödinger equation to the complex $\mathbf{k}$ space.[15] In application to semi-infinite systems, we use the ELAPW-$\mathbf{k}\cdot\mathbf{p}$ method to solve the *inverse band-structure problem*: given two real Cartesian components of the Bloch vector $\mathbf{k}^{\parallel} = (k_x, k_y)$ and the energy $E$, we find the values of $k^{\perp}$ that satisfy the Schrödinger equation

$$\hat{H}\Psi(E, \mathbf{k}^{\parallel} + \mathbf{z}k_n^{\perp}; \mathbf{r}) = E\Psi(E, \mathbf{k}^{\parallel} + \mathbf{z}k_n^{\perp}; \mathbf{r}) \qquad (1)$$

for the Bloch vector with a complex $z$-component $k_n^{\perp}$ ($\mathbf{z}$ is a unity vector in the $z$-direction).

In the $\mathbf{k}\cdot\mathbf{p}$ method the wave function of a Bloch vector $(\mathbf{k}^{\parallel} + \mathbf{z}k^{\perp})$ is a product of a trial function with the Bloch vector $(\mathbf{k}^{\parallel} + \mathbf{z}k_0^{\perp})$ and the phase factor $\exp[i(k^{\perp} - k_0^{\perp})z]$. The trial function is a linear combination of the basis functions $\xi_j(\mathbf{k}_0; \mathbf{r})$ constructed at the reference point $\mathbf{k}_0 = \mathbf{k}^{\parallel} + \mathbf{z}k_0^{\perp}$ with a real $k_0^{\perp}$:

$$\Psi(E, \mathbf{k}^{\parallel} + \mathbf{z}k^{\perp}; \mathbf{r}) = e^{\,i(k^{\perp} - k_0^{\perp})z} \sum_j C_j^{k^{\perp}}(E, \mathbf{k}_0)\ \xi_j(\mathbf{k}_0; \mathbf{r}).$$

In terms of the coefficient vectors $\vec{C}_n \equiv \{C_j^{k_n^\perp}\}$ the inverse problem can be written as a matrix equation

$$\left[\hat{H} + 2\delta_n^\perp \hat{P}^\perp + ({\delta_n^\perp}^2 - E)\,\hat{O}\right]\vec{C}_n = 0, \qquad (2)$$
$$\delta_n^\perp = k_n^\perp - k_0^\perp,$$

with $\hat{H}$ being the Hamiltonian, $\hat{O}$ the overlap matrix, and $\hat{P}^\perp$ the $z$-projection of the momentum matrix. By introducing the vector $\vec{D}_n = -(2\hat{P}^\perp + \delta_n^\perp \hat{O})\,\vec{C}_n$ we reduce Eq. (2) to a linear eigenvalue problem of twice the dimension:

$$\begin{pmatrix} 0 & \hat{H} - E\hat{O} \\ \hat{I} & 2\hat{P}^\perp \end{pmatrix}\begin{pmatrix} \vec{D}_n \\ \vec{C}_n \end{pmatrix} = \delta_n^\perp \begin{pmatrix} \hat{I} & 0 \\ 0 & -\hat{O} \end{pmatrix}\begin{pmatrix} \vec{D}_n \\ \vec{C}_n \end{pmatrix}. \qquad (3)$$

Thus, the solutions of the inverse band-structure problem $k_n^\perp$ are obtained as the eigenvalues $\delta_n^\perp$ of this generalized non-Hermitian problem.

Because of the rather large unit cell of $NbSe_2$ (six atoms per unit cell) the solution of Eq. (3), especially for complex matrices, results in prohibitively time-consuming calculations.[28] It has turned out that the CPU time can be greatly reduced by orthogonalizing the original basis set, i.e., by seeking the trial function in terms of the bulk Hamiltonian eigenfunctions $\psi_j(\mathbf{k}_0;\mathbf{r})$ at $\mathbf{k}_0$ rather than in terms of the basis functions $\xi_j(\mathbf{k}_0;\mathbf{r})$. Eliminating the overlap matrix alone makes the computing of Eq. (3) three times faster. The price for that is the necessity of recalculating the momentum matrix $\hat{P}^\perp$, which scales quadratically with the number of both basis functions and eigenfunctions. To further accelerate the procedure we cut the eigenvalue spectrum and retain only $\psi_j$ with energies lower than 5 Ryd above the spectral interval we are interested in. A suitable cutoff energy is difficult to determine *a priori*, however, the quality of the results can be verified by comparing the resulting inverse band structure $k^\perp(E)$ with the usual band structure $E(k^\perp)$.

### B. Constructing the LEED Function

In the bulk half-space the LEED function $\Phi$ is expanded in terms of the solutions $\Psi_n \equiv \Psi(E, \mathbf{k}^\parallel + \mathbf{z}k_n^\perp; \mathbf{r})$ of Eq. (3). The quality of the wave functions $\Psi_n$ is known to deteriorate with growing $|\delta_n^\perp|$.[15] With the present computational setup reliable solutions were found to be restricted to the interval $\mathrm{Im}\,\delta_n^\perp < 3$ Å$^{-1}$. To construct the LEED function, we take all the solutions in this interval, which for $NbSe_2$ is typically ten (at the vacuum level $E_{\mathrm{vac}}$) to twenty Bloch waves (at 40 eV above $E_{\mathrm{vac}}$). Then a Laue representation of the functions is constructed

$$\Psi_n(\mathbf{r}^{||}, z) = \sum_{s=0}^{N_F-1} f_{sn}(z)\exp\left[\,i(\,\mathbf{k}^{||} + \mathbf{G}_s^{||}\,)\,\mathbf{r}^{||}\,\right]. \qquad (4)$$

Here $\mathbf{r}^{||} = (r_x, r_y)$ and $\mathbf{G}_s^{||}$ are surface reciprocal vectors. To construct the Laue representation we use a rapidly converging 3D Fourier decomposition of the wave function, which differs from the true all-electron wave function only in a close vicinity of the nucleus (see the gouging technique described in Refs. 24 and 29). Each surface Fourier component $f_{sn}(z)$ is smoothly continued into the vacuum half-space by a linear combination of two plane waves, one of which is the outgoing vacuum solution $\exp[\,ik_s z\,]$ with $|\,\mathbf{k}^{||} + \mathbf{G}_s^{||}\,|^2 + k_s^2 = E$, and the other one is a decaying (unless $\mathbf{G}_s^{||} = 0$) plane wave $\exp[\,iq_s z\,]$ with a purely imaginary $z$-component $q_s$. In the present calculation it has been chosen $k_s^2 - q_s^2 = \Delta E$ for all $s$ with $\Delta E = 3$ Ryd. For $\mathbf{G}_0^{||} = 0$ one of the waves represents the incident electron wave, and the other one the reflected wave, i.e., $q_0 = -k_0$.

Thereby the functions $\Psi_n$ are defined in the whole space and they are smoothly continuous everywhere. The LEED function $\Phi$ is sought as a linear combination of the functions that minimizes the value

$$\|(\hat{H} - E)\Phi\| = \int\limits_{\mathrm{vacuum}} |(\hat{H} - E)\Phi(\mathbf{r})|^2\, d\mathbf{r}, \qquad (5)$$

under the constraint that the incident current is equal to unity. The resulting function $\Phi(\mathbf{r})$ is the closest to a solution of the Schrödinger equation in the surface region. By construction the trial function satisfies the Schrödinger equation both in the bulk half-space and far from the surface in the vacuum, so that only a finite slab in the vicinity of the surface contributes to the integral (5). This slab may include the part of the crystal where the potential strongly deviates from the bulk potential, but in this calculation we adopt a simplified step-like shape of the surface barrier, so the potential changes abruptly in the middle of the van-der-Waals gap from its bulk distribution to the constant vacuum value. The generalization of the method to the case of an arbitrary potential in the interface region has been described in Ref. 30.

The minimization procedure $\delta\|(\hat{H} - E)\Phi\| = 0$ leads to a system of linear equations. If the auxiliary tails $\exp[\,iq_s z\,]$ accidentally cancel then the result is equivalent to the simple matching of wave functions. It is, however, difficult to predict whether the matching is possible and to separate the matching error from the errors introduced at the stage of obtaining the LEED function constituents $\Psi_n$.[15] If the exact matching is impossible the variational method yields a solution that is smoothly continuous by construction – this function is thought to be the best approximation for the LEED function we seek. The accuracy of the ultimate result can be estimated *a posteriori* by checking the current conservation in the LEED function, i.e., by comparing the current transmitted into the crystal by the superposition of the propagating Bloch waves $\Psi_n$ to the current in the vacuum carried by the superposition of plane waves.

### C. Normal Incidence Spectrum

The $\mathbf{k}^{||} = 0$ spectra along with the underlying real band structure are presented in Fig. 2. The $V_{\rm i} = 0$ calculation yields partial currents carried by the Bloch states (shown by whiskers). It reveals the conducting states responsible for the transmission of the current, thereby offering an interpretation of the VLEED spectrum in terms of conducting fragments of the band structure: the abrupt changes in $T(E)$ all reflect critical points in the conducting bands.

The deviation of the $k^{\perp}(E)$ points by the inverse ELAPW-$\mathbf{k}\cdot\mathbf{p}$ from the $E(k^{\perp})$ lines by the direct method with the full basis is seen to be negligible. Together with the reasonably small current non-conservation this justifies the basis set reduction we have undertaken to make the calculations feasible.

A special feature of the normal incidence spectrum is that the conducting bands do not overlap, i.e., there is only one dominant propagating constituent in the LEED function. In this respect the picture is similar to that of the Slater 1D model.[7] The inclusion of the imaginary term lifts the principal difference between the propagating and evanescent waves (whose properties to couple to the incoming wave may be very similar) and thereby levels out the intensity variations (see the dashed curve in Fig. 2). In particular, already at a moderate value of $V_{\rm i} = 0.5$ eV the narrow gaps in the $T(E)$ spectrum almost completely disappear, so one can hardly expect them to be observed in the experiment. Wider gaps remain well visible, although the reflected intensities are strongly reduced and the structures broadened with respect to those predicted by a Hermitian Hamiltonian. In the next section we will use these properties of the Slater theory to extract quantitative information about the damping of quasi-particles from the shape of experimental spectra.

## V. DETERMINING THE ENERGY DEPENDENCE OF $V_{\rm i}$

We shall now compare our measured target current spectra $I(E)$ with the calculated transmission coefficient $T(E)$. First of all, we need to bring the $I(E)$ spectrum to the same absolute units as $T(E)$. This is not trivial because of the presence of the unknown background caused by the secondary electrons contributing to the reflectivity. In view of the close similarity of the fine structure of the measured $I(E)$ and theoretical $T^{\rm th}(E)$ spectra over a wide energy region, see Fig. 3, we have chosen to determine the *experimental* $T(E)$ curve by fitting $I(E)$ to $T^{\rm th}(E)$ with the linear transformation $T^{\rm exp}(E) = aI(E) + b + cE$. Here the function $b + cE$ represents a linearly varying background.

Strong intensity variations in the $T(E)$ spectrum are much more important for the band structure information than the shape of the maxima,[3] which are very broad even if the damping is neglected (see Fig. 2). Thus, for a conclusive comparison, the extrema of the $dT(E)/dE$ function must be analyzed.

Owing to computational instabilities, theoretical $T(E)$ curves contain numerical noise, which should be excluded before the derivative is calculated. To remove the jaggedness we average the $T(E)$ function within an interval of width $\Delta E$ by fitting it to a parabola: for a given $E$ a parabola is constructed that approximates the raw $T(E)$ spectrum over the interval $[E-\Delta E/2; E+\Delta E/2]$ and its value at $E$ is taken to be the intensity of the smoothed $T(E)$ spectrum. The width $\Delta E$ of the interval is 0.6 eV at the vacuum level and it grows linearly up to 2.4 eV at 50 eV above $E_{\rm vac}$. Thereby slow changes of intensity are not affected and only the noise is removed.

We extract the energy dependence of the optical potential $V_{\rm i}(E)$ from the experimental spectra by comparing the sharpness of the $dT/dE$ extrema (maxima and minima) in the experimental and theoretical spectra. To quantitatively characterize the sharpness, we associate the function $dT/dE$ in the interval between its two zeros $E_1$ and $E_2$ with a parabola that passes through zero at $E_1$ and $E_2$ and embraces the same area $S$ as the $dT/dE$ function, $S = T(E_2) - T(E_1)$. Then the curvature of the parabola $6S/(E_2-E_1)^3$ is taken to express the sharpness of the structure. This parameter changes very strongly over the spectrum, so in Fig. 4 we show the cube root of the curvature $\sqrt[3]{S}/(E_2-E_1)$. We have performed a series of calculations for the normal incidence with an energy independent $V_{\rm i}$ ranging from 0.5 to 3 eV and considered the sharpness of each structure as a function of optical potential. Three examples are shown in the right panel of Fig. 4. The value of sharpness from the left panel is taken to yield the value of the optical potential in the right panel. One immediately notices a sharp increase of the optical potential between 16 and 21 eV: the two minima change their shape very similarly with increasing the $V_{\rm i}$ (circles and diamonds in right panel of Fig. 4) and the minimum at 21 eV in the experiment is significantly broader than the one at 16 eV (see left panel of Fig. 4).

The values of $V_{\rm i}$ determined in this way are necessarily overestimated. First, in addition to the inelastic processes in the electronic system, there exist broadening mechanisms dependent upon experimental conditions, such as surface roughness and finite energy resolution. Also the angular spread of the incident beam contributes to the broadening owing to the $\mathbf{k}^{\parallel}$ dispersion of spectral structures. Secondly, our theoretical spectra do not take into account inelastic scattering in the surface barrier region, e.g., scattering on the surface defects. This effect results in an additional reduction of the spectral structures but, unlike the inelastic scattering in the bulk, it hardly affects their energy broadening. These mechanisms should, however, be less significant for the layered materials because of the rather small electron density at the surface and a small concentration of defects on the cleaved surface. On the other hand, our absolute values of $V_{\rm i}$ are in accord with the recent *ab initio* results

on the quasi-particle lifetimes for noble and transition metals:[31] For energies around $E - E_F = 5$ eV the calculated lifetimes do not exceed a few fs ($V_\mathrm{i} \sim 0.2 - -0.7$ eV).

The energy dependence $V_\mathrm{i}(E)$ derived from the experiment is presented in Fig. 5. To get an idea of how reliable the obtained $V_\mathrm{i}(E)$ dependence is we compare the normal incidence data (circles) with the data for $\mathbf{k}^{||} = \frac{1}{4}\Gamma\mathrm{K}$ ($\times$). (The off-normal incidence spectra are shown in Fig. 6; $\frac{1}{4}|\Gamma\mathrm{K}| = 0.3$ Å). The absolute values of $V_\mathrm{i}$ agree very well and both spectra suggest a sharp increase at around 20 eV. The non-steady behavior of the $\mathbf{k}^{||} = \frac{1}{4}\Gamma\mathrm{K}$ derived values around 30 eV seems to have no physical meaning; it reflects the disagreement between theory and experiment in shape of the $T(E)$ maximum at 25 eV, which in section VI we explain by the deviation of the calculated band structure from the experimentally observed one.

An optical potential is associated with the imaginary part of the electron self-energy $\Sigma$, whose energy dependence is expected to reflect singularities of the energy loss function $-\mathrm{Im}[1/\varepsilon(\mathbf{q},\omega)]$. In particular, in the *GW* approximation,[32] $\mathrm{Im}\,\Sigma$ is given by an integral, whose integrand contains the inverse dielectric function (DF). We are not in a position to calculate the lifetime of the LEED constituents *ab initio*. A rough idea of the average effect of plasmon excitations on the energy dependence of the electron lifetime can be obtained from the DF for $\mathbf{q} = 0$ by plotting the integral $\int_0^E -\mathrm{Im}[1/\varepsilon(\mathbf{q} = 0, \omega)]\, d\omega$. We have calculated the DF in the random phase approximation, see Sec. VII. In Fig. 5 we compare the integral function to the experimental dependence $V_\mathrm{i}(E)$. The sharp increase of the optical potential agrees well with the plasmon location at 21 eV (see also Fig. 11 in Sec. VII), which is confirmed by the transmission energy loss measurements by Bell and Liang.[33] Our theoretical DF shows also a second plasmon peak at 35 eV, which may be responsible for the step-like growth of the optical potential at higher energies.

## VI. ΓK DIRECTION

Experimental and theoretical $T(E)$ curves for $\mathbf{k}^{||}$ ranging from zero to ΓK are presented in Fig. 6. The experimental and theoretical spectral structures show a good agreement in both energy dispersion and relative amplitudes. Owing to the increase of the incident beam spread in $\mathbf{k}^{\|}$, the low-energy part of the experimental spectra at large $\mathbf{k}^{\|}$ looks smeared compared to the theory. Note that because of the vector $\mathbf{k}^{||}$ changing with the incident electron energy the spectra cannot be compared in a one-to-one manner. To facilitate the comparison of the dispersion of the spectral structures we present a gray-scale $T(\mathbf{k}^{||}, \mathbf{E})$ plot, Fig. 7. A very good agreement between the measured and calculated $\mathbf{k}^{||}$ dispersion of the $T(E)$ intensity proves that the theoretical approach we have adopted is adequate. The results have turned out rather sensitive to details of the potential distribution in the bulk half-space; we stress that the advantage of the ELAPW-$\mathbf{k}\cdot\mathbf{p}$ method of accurately taking into account the strong non-muffin-tin effects makes the method an indispensable tool for studying the electron diffraction on layered materials.

We now analyze the information on the bulk band structure contained in our experimental data (and deliberately blurred by the optical potential in the theory). The critical points in the $k^{\perp}$ dispersion of the conducting bands (e.g. the band edges) manifest themselves as the extrema in the $dT/dE$ curve. Of course, reflected is the optical-potential-damped (completely complex) band structure, in which the band dispersions are smoothed, and the critical points are shifted by some tenth of eV from their $V_\mathrm{i} = 0$ positions.[1] The deviation of the surface barrier from the step-like form may also cause shifts of $dT/dE$ extrema, but for the layered material this effect seems to be insignificant.

To stress the $\mathbf{k}^{\|}$ dispersion of the spectral structures we construct a gray-scale plot, Fig. 8, in which the shading shows the energy area covered by the conducting bands (the regions between $dT/dE$ maxima and minima); $\mathbf{k}^{||}$ projected band gaps then appear as white areas. Again one observes excellent overall agreement between the experiment and theory. The plot, however, reveals also differences in finer details, which reflects fundamental limitations of the theory employing a one-electron band structure and optical potential. The deviations are necessarily present due to our neglect of the real part of the self-energy $\Sigma(E, \mathbf{k})$ – it is replaced by an exchange-correlation potential in the local density approximation. For example, the white area ranging from $\mathbf{k}^{||} = 0$, $E - E_F = 27$ eV to $\mathbf{k}^{||} = 0.7$ Å$^{-1}$, 31 eV in the experiment is shifted towards higher energies by about 1 eV with respect to its calculated counterpart. In particular, this causes the higher width of the measured $T(E)$ maxima between 25 and 29 eV than in the theory (see the discussion in Sec. V). The difference is especially well visible between 0.2 and 0.4 Å$^{-1}$. The discrepancies are seen to significantly increase above ∼40 eV: an overall shift of the experimental bands to higher energies is observed.

The deviations are seen to increase at larger $\mathbf{k}^{\|}$. From the band-structure point of view the main difference between the normal and off-normal incidence spectra is that in the latter case the conducting bands intersect; in other words the LEED state contains more than one propagating Bloch constituent. An example for $\mathbf{k}^{\|} = \Gamma\mathrm{K}$ is shown in Fig. 9, lower panel. The theoretical $T(E)$ curve for negligible absorption (solid line) has a different character from the normal incidence spectrum (Fig. 2): there are no energy gaps in the band structure along the KH line, and the transmission never drops to zero and never reaches unity – it almost never exceeds 0.8. Thus, not only minima but also maxima are affected by the optical potential. Also the positions of spectral minima strongly depend upon the function $V_\mathrm{i}(E)$. For example, with increasing $V_\mathrm{i}$, the minimum at 19.6 eV moves away

from its measured location towards lower energies and in the spectrum calculated with the energy dependent $V_\mathrm{i}$ it appears at 17.9 eV. Such a high sensitivity of results to a phenomenological parameter may be an important limitation of the theory. Although the overall shape of the $\mathbf{k}^\parallel = \Gamma\mathrm{K}$ spectrum is well reproduced by the theory, the band structure information may be incorrectly transferred to the $T(E)$ curve.

Presumably, the weak point is the presence of several propagating Bloch waves in the band-structure decomposition of the LEED function. In connecting the optical potential to the electron attenuation we basically rely on the relation $\mathrm{Im}\, k^\perp \sim V_\mathrm{i}/v^\perp$. The parameter $V_\mathrm{i}$ is, thus, easy to operate when there is only one wave, but its meaning is not that transparent when there are several waves with different velocities (which, in addition, are connected by the matching conditions). This point of view is supported by Fig. 10 in which we compare the measured $\mathbf{k}^\parallel$ dispersion of the $T(E)$ minima with theoretical results for the energy dependent $V_\mathrm{i}$ and for a constant moderately small $V_\mathrm{i}$ of 0.5 eV. The latter results are expected to provide undistorted information on the band structure. One can see that whenever there is a disagreement between small $V_\mathrm{i}$ and large $V_\mathrm{i}$ results, for small $k^\parallel$ the experimentally determined function $V_\mathrm{i}(E)$ brings the positions of the minima closer to the experiment (areas A and B). On the contrary, for large $k^\parallel$ the $V_\mathrm{i} = 0.5$ eV results are often closer to the experiment (areas C and D).

Such deviations can be corrected by introducing a position dependent (in general non-local) $V_\mathrm{i}$, which would allow to control the behavior of the complicated LEED state. In this case different Bloch constituents would be damped differently depending on their spatial distributions. Such an approach within the multiple-scattering formalism of VLEED has been developed by Bartoš *et al.* in Ref. 34.

## VII. OPTICAL PROPERTIES

Optical properties of the crystal provide independent information on the unoccupied band structure. Within the one-particle theory – random phase approximation[35] without local field effects – the calculations employ the same unoccupied bulk states as the LEED calculations of Sec. IV A.

The imaginary part of the dielectric function $\varepsilon_2(\omega)$ was calculated as an integral over the BZ with the tetrahedron method (for computational parameters see Sec. III). The real part $\varepsilon_1(\omega)$ was determined out of $\varepsilon_2(\omega)$ by the Kramers-Kronig integration with the energy cutoff $\hbar\omega_{\max} = 70$ eV [The values of $\varepsilon_2(\omega)$ above 38 eV are underestimated because of the finite number of bands taken into account – from Nb $4p$ (-31 eV) up to 38 eV above the Fermi level.]

In Fig. 11 we compare our *ab initio* results with the reflectivity measurements by Liang[36] and transmission energy loss spectrum by Bell and Liang.[33] The experimental data are in excellent agreement with the calculations. The main plasmon peak at 21 eV corresponds to the termination of transitions from the $4d$ valence band states. Our calculations predict also a rather strong peak at 36 eV due to the transitions from the semi-core Nb $4p$ states to the unoccupied Nb $4d$ peak at $E - E_F = 3$ eV (see Fig. 1). The high-energy plasmon is important to understand the energy dependence of the electron lifetime.

## VIII. CONCLUSIONS

Angle-dependent VLEED measurements in the target current mode have been performed on the layered 2H-$NbSe_2$. Tight control over the electron beam and adjustment of the incidence angle in three angular degrees of freedom enabled highly accurate measurements for the incidence wave vector $\mathbf{k}^\parallel$ scanning the ΓK line of the Brillouin zone. Based on the self-consistent band structure, *ab initio* VLEED spectra have been calculated with the ELAPW-$\mathbf{k}\cdot\mathbf{p}$ method, the inelastic scattering being modelled via the optical potential.

A novel methodological aspect is the algorithm to extract the information on the electron lifetime from the VLEED experiment. The obtained results are consistent with available experimental and theoretical information on the dielectric function of $NbSe_2$.

Owing to the complicated non-free-electron-like unoccupied band structure of $NbSe_2$, the VLEED spectra show rich structure over the energy region up to 50 eV above the Fermi level. A good agreement between experiment and theory in the energy location of the TCS structures over the whole interval makes it possible to interpret the observed shape of the spectra in terms of the energy dependent optical potential.

The comparison of the experimental and theoretical results focusses on the surface-projected band structure represented by the $\mathbf{k}^\parallel$ dispersion of the extrema in the energy derivative of the transmission coefficient $dT/dE$. A good agreement between the experiment and theory proves that our theoretical approach is capable of accurate description of the unoccupied bands of $NbSe_2$. Minor discrepancies have been observed, which are traced back to the imperfectness of our one-electron approach as well as to intrinsic shortcomings of the phenomenological treatment of inelastic scattering.

## ACKNOWLEDGMENTS

The authors benefited from discussions with I. Bartoš. We acknowledge the support of Deutsche Forschungsgemeinschaft to E.E.K. (Forschergruppe DE 412/21), and to V.N.S. and R.C. (CL124/5-1).

† Also with the Institute for High-Performance Computations and Data Bases, P. O. Box 71, 194291 St.Petersburg, Russia

[1] V. N. Strocov, H. Starnberg, and P. O. Nilsson, J. Phys.: Cond. Matter **8**, 7539 (1996).
[2] V. N. Strocov, H. Starnberg, P. O. Nilsson, H. E. Brauer, and L. J. Holleboom, Phys. Rev. Lett. **79**, 467 (1997); J. Phys. Condens. Matter **10**, 5749 (1998).
[3] V. N. Strocov, R. Claessen, G. Nicolay, S. Hüfner, A. Kimura, A. Harasawa, S. Shin, A. Kakizaki, H. I. Starnberg, P. O. Nilsson, and P. Blaha, Phys. Rev. Lett. **81**, 4943 (1998); Phys. Rev. B **63**, 205108 (2001).
[4] J.-V. Peetz, W. Schattke, H. Carstensen, R. Manzke, and M. Skibowski, Phys. Rev. B **46**, 10127 (1992).
[5] P. J. Feibelman, and D. E. Eastman, Phys. Rev. B **10**, 4932 (1974).
[6] *Angle-Resolved Photoemission*, edited by S. D. Kevan (Elsevier, Amsterdam, 1992).
[7] J. C. Slater, Phys. Rev. **51**, 840 (1937).
[8] V. N. Strocov, P. Blaha, H. I. Starnberg, M. Rohlfing, R. Claessen, J.-M. Debever, and J.-M. Themlin, Phys. Rev. B **61**, 4994 (2000); V. N. Strocov, A. Charrier, J.-M. Themlin, M. Rohlfing, R. Claessen, N. Barrett, J. Avila, J. Sanchez, and M.-C. Asensio, Phys. Rev. B **64**, 075105 (2001).
[9] E. Pehlke and W. Schattke, *Solid State Commun.* **69**, (1989) 419.
[10] V. N. Strocov, in *Electron spectroscopies applied to low-dimensional materials* (Kluwer, Netherlands, 2000)
[11] G. Wachutka, Phys. Rev. B **34** 8512 (1986).
[12] W. Hummel and H. Bross, Phys. Rev. B **58** 1620 (1998).
[13] M. D. Stiles and D. R. Hamann, Phys. Rev. B **38**, 2021 (1988).
[14] D. Wortmann, H. Ishida, and S. Blügel, Phys. Rev. B **65**, 165103 (2002).
[15] E. E. Krasovskii and W. Schattke, Phys. Rev. B **56**, 12874 (1997).
[16] R. Corcoran, P. Meeson, Y. Onuki, P-A. Probst, M. Springford, K. Takita, H. Harima, G. Y. Guo, and B. L. Gyorffy, J. Phys.: Condens. Matter **6** 4479 (1994).
[17] Th. Straub, Th. Finteis, R. Claessen, P. Steiner, S. Hüfner, P. Blaha, C. S. Oglesby, E. Bucher, Phys. Rev. Lett. **82**, 4504 (1999).
[18] T. Yokoya, T. Kiss, A. Chainani, S. Shin, M. Nohara, and H. Takagi, Science **294**, 2518 (2001)
[19] V. N. Strocov, Th. Finteis, R. Claessen, G. Nicolay, D. Ehm, V. Colbus, S. Hüfner, H. Starnberg, and V. Eyert, *BESSY Annual Rep.*, 219 (1997).
[20] K. Rossnagel, O. Seifarth, L. Kipp, M. Skibowski, D. Voss, P. Krüger, A. Mazur, and J. Pollmann, Phys. Rev. B **64**, 235119 (2001).
[21] V. N. Strocov, Meas. Sci. Technol. **7**, 1636 (1996).
[22] We thank F. Lévy for deposition of the phosphor film.
[23] S. A. Komolov, *Total Current Spectroscopy of Surfaces* (Gordon and Breach, Philadelphia, 1992).
[24] E. E. Krasovskii, F. Starrost, and W. Schattke, Phys. Rev. B **59**, 10504 (1999).
[25] E. E. Krasovskii and W. Schattke, Phys. Rev. B **63**, 235112 (2001).
[26] G. K. Wertheim, F. J. DiSalvo, and D. N. E. Buchanan, Solid State Commun. **13** 1225 (1973).
[27] D. S. Boudreaux and V. Heine, Surf. Sci. **8**, 426 (1967); J. B. Pendry, J. Phys. C **2**, 2273 (1969).
[28] Each energy point takes 25 min CPU time of ALPHA 21264 EV6 (500 MHz).
[29] E. E. Krasovskii and W. Schattke, Phys. Rev. B **60**, 16251 (1999).
[30] E. E. Krasovskii and W. Schattke, Phys. Rev. B **59**, 15609 (1999); Czechoslovak Journal of Physics, **49**, 1575 (1999).
[31] V. P. Zhukov, F. Aryasetiawan, E. V. Chulkov, I. G. de Gurtubay, and P. M. Echenique, Phys. Rev. B **64**, 195122 (2001); V. P. Zhukov, F. Aryasetiawan, E. V. Chulkov, and P. M. Echenique, *ibid.* **65**, 115116 (2002).
[32] L. Hedin and S. Lundqvist, in *Solid State Physics*, edited by F. Seitz, D. Turnbull, and H. Ehrenreich, **23**, (Academic press, New York, 1969), p.1.
[33] M. G. Bell and W. Y. Liang, Adv. Phys. **25**, 53 (1976).
[34] I. Bartoš, M. A. Van Hove and M. S. Altmann, Surf. Sci. **352-354**, 660 (1996).
[35] H. Ehrenreich and M. A. Cohen, Phys. Rev. **115**, 786 (1959).
[36] W. Y. Liang, J. Phys.C: Solid State Phys. **6** 551 (1972).

FIG. 1. Density of states for $NbSe_2$: total DOS (solid line) and $l$-projected Nb $d$ (dot-dashed line) and Se $p$ (dotted line) partial DOS per atom. (Note the energy scale break at 7 eV.) Dashed curve shows the X-ray photoemission spectrum by Wertheim *et al.*[26]

FIG. 2. Calculated unoccupied band structure of $NbSe_2$ in the ΓA direction. The lines in the left panel show the band structure $E(k^{\perp})$ for $V_{\rm i} = 0$ obtained with the direct ELAPW-$\mathbf{k}\cdot\mathbf{p}$ method (without the basis reduction). The conducting bands are marked by whiskers, whose upper ends show the band structure $k^{\perp}(E)$ obtained with the inverse method. The length of the whisker is proportional to the contribution of the Bloch wave to the target current. Transmission coefficient $T(E)$ (calculated in the vacuum half-space) is shown in the right panel by the solid line. The shaded area shows its deviation from the current in the bulk (the sum of the group velocities times the weights with which the constituents enter the LEED function). The dashed line is the $T(E)$ spectrum with the optical potential $V_{\rm i} = 0.5$ eV added to the Hamiltonian $\hat{H}$ in Eq. (3).

FIG. 3. Comparison of the normal incidence target current $I(E)$ and transmission coefficient $T(E)$ spectra of $NbSe_2$. The measured $I(E)$ curve is shown by the dot-dashed line. Theoretical $T(E)$ and $dT/dE$ spectra are shown by dashed lines in the lower and upper panels respectively; they are calculated with an energy dependent optical potential [the $V_i(E)$ function is shown in Fig. 5]. To arrive at the experimental $T(E)$, the original $I(E)$ function is fitted to the theoretical $T(E)$ by a linear transformation that involves scaling and subtracting the background. The resulting experimental $T(E)$ and $dT/dE$ curves are shown by solid lines.

FIG. 4. Left panel: sharpness of the extrema in the experimental ($\times$) and theoretical ($\circ$) $dT/dE$ spectra (see upper panel of Fig. 3). Negative values are ascribed to minima and positive to maxima. Right panel: dependence of the sharpness upon the optical potential for two minima (at 16 and 21 eV) and a maximum (at 30 eV) in the $dT/dE$ spectrum.

FIG. 5. Dependence of the optical potential $V_i$ on the incident electron energy extracted from the normal ($\circ$) and an off-normal ($\times$) incidence spectrum. The function $V_i(E)$ used in the calculations is shown by the dashed line. The solid line is the function $\int_0^E -\mathrm{Im}[1/\varepsilon(\mathbf{q}=0,\omega)]\; d\omega$.

FIG. 6. Experimental (left) and theoretical (right) angular dependence of the $T(E)$ spectra with the vector $\mathbf{k}^{||}$ scanning the ΓK line of the BZ. In the experiment the sample rotation angle $\alpha$ increases in steps of $0.5^\circ$. The onsets of the spectra are at the energy $e\varphi + (\hbar^2/2m)K_\parallel^2$ at which the electrons start penetrating into the solid. Owing to the retarding field, the incidence angle differs from $\alpha$ and depends on energy in such a way that $\mathbf{k}^{\parallel}$ varies along the spectrum almost linearly. In the left panel the $\mathbf{k}^{\parallel}$ values are indicated that correspond to the onset of the spectrum and to $E - E_F = 50$ eV. Note the scale change at 18.5 eV (marked by a dashed line).

FIG. 7. Experimental (left) and theoretical (right) $\mathbf{k}^{\parallel}$ distribution of the $T(E)$ spectral intensity shown in a linear gray scale. White areas correspond to maximal $T(E)$. [Original $T(E)$ curves are shown in Fig. 6]. The energy region shown begins 0.5 eV above the transmission onset. Note the scale change at 18.5 eV (marked by a white line).

FIG. 8. Experimental (left) and theoretical (right) $\mathbf{k}^{\parallel}$ dispersion of the $dT/dE$ spectra. [Original $T(E)$ curves are shown in Fig. 6]. The shading fills the regions between the maxima and minima in the $dT(E)/dE$ spectra, i.e., the area where the second derivative $d^2T/dE^2$ is negative. Physically, the shaded area shows the surface-projected dispersion $E(\mathbf{k}^{\parallel})$ of the conducting bands. The gray scale shows the amplitude of $d^2T/dE^2$ (in a logarithmic scale), which characterizes the amplitude and sharpness of the extrema. The shown energy region begins 0.5 eV above the transmission onset.

FIG. 9. Dependence of the electron transmission spectrum for $\mathbf{k}^{\parallel} = \Gamma\mathrm{K}$ on the optical potential. Experimental spectrum is shown by the dashed line. In the lower panel conducting fragments of the band structure in the H-K-H interval are shown (see also the caption of Fig. 2)

FIG. 10. $\mathbf{k}^{\parallel}$ dispersion of $T(E)$ minima: experiment (dots); theory with the energy dependent $V_i$ (circles) and with $V_i = 0.5$ eV (lines).

FIG. 11. Optical properties of $NbSe_2$ for two light polarizations: $\mathbf{E} \perp \mathbf{c}$ (solid lines) and $\mathbf{E} \parallel \mathbf{c}$ (dashed lines). The experimental reflectivity spectrum[36] for $\mathbf{E} \perp \mathbf{c}$ is shown in the upper panel by the dot-dashed line. The triangles in the lower panel show the energy location and intensity of the low-energy structures of the measured[33] EELS spectrum. The fragment of the Lorentzian function (dotted line) reproduces the experimentally observed[33] energy location, intensity, and width of the main plasmon.

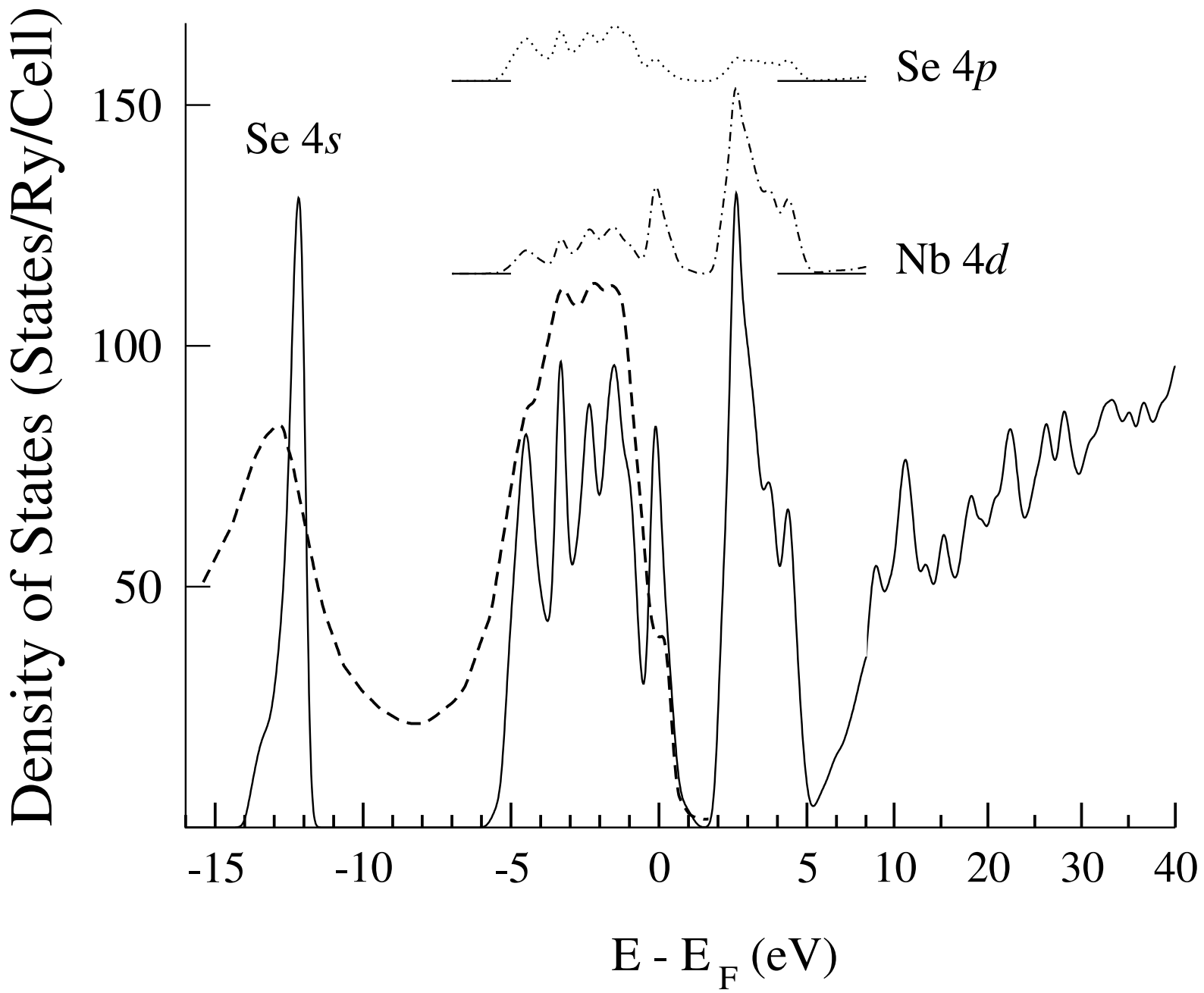
Density of States (States/Ry/Cell)
150
100
50
Se 4s
Se 4p
Nb 4d
-15
-10
-5
0
5
10
20
30
40
E - E F (eV)

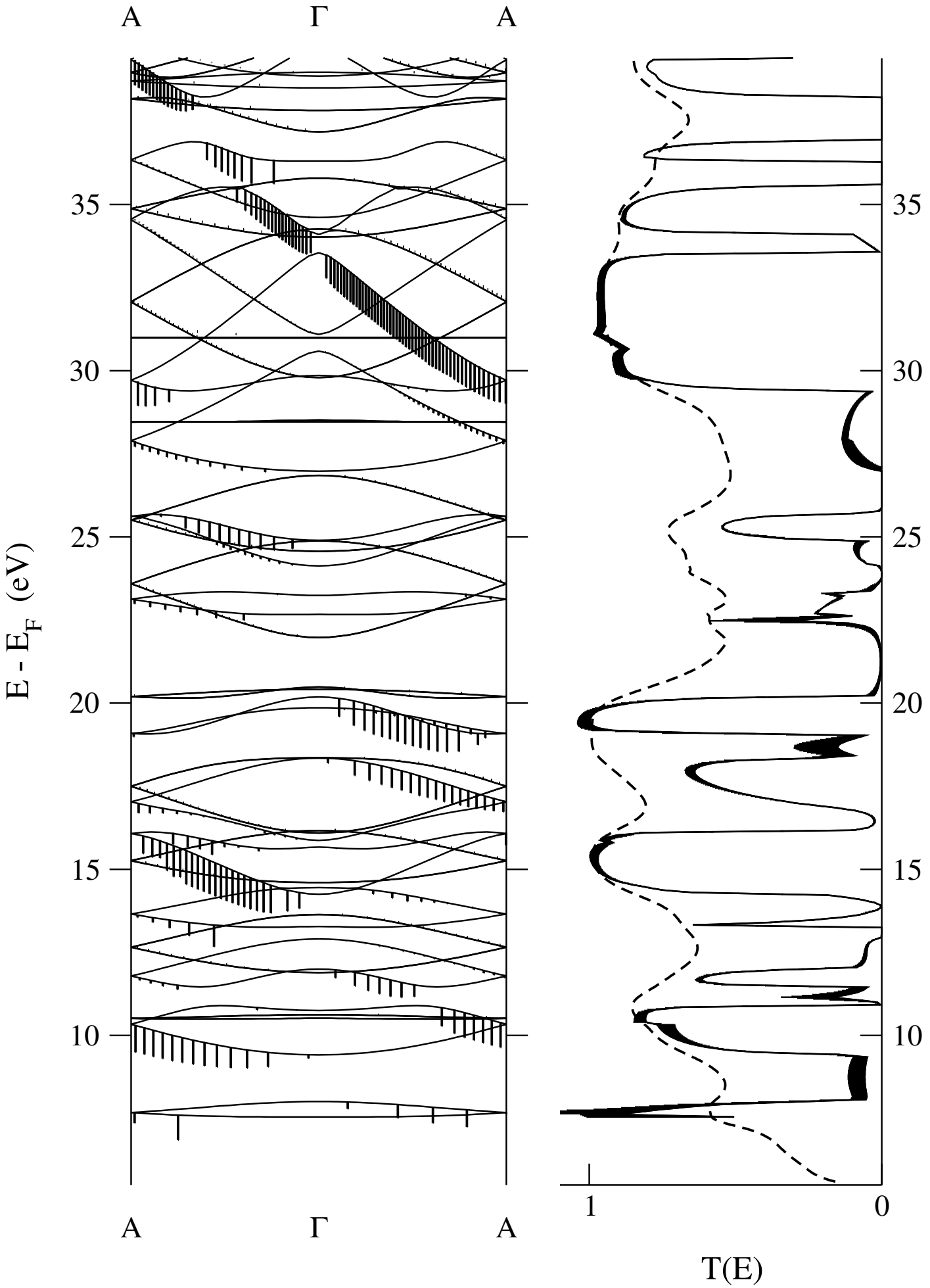
A
Γ
A
35
30
25
20
15
10
E - E_F (eV)
1
0
T(E)

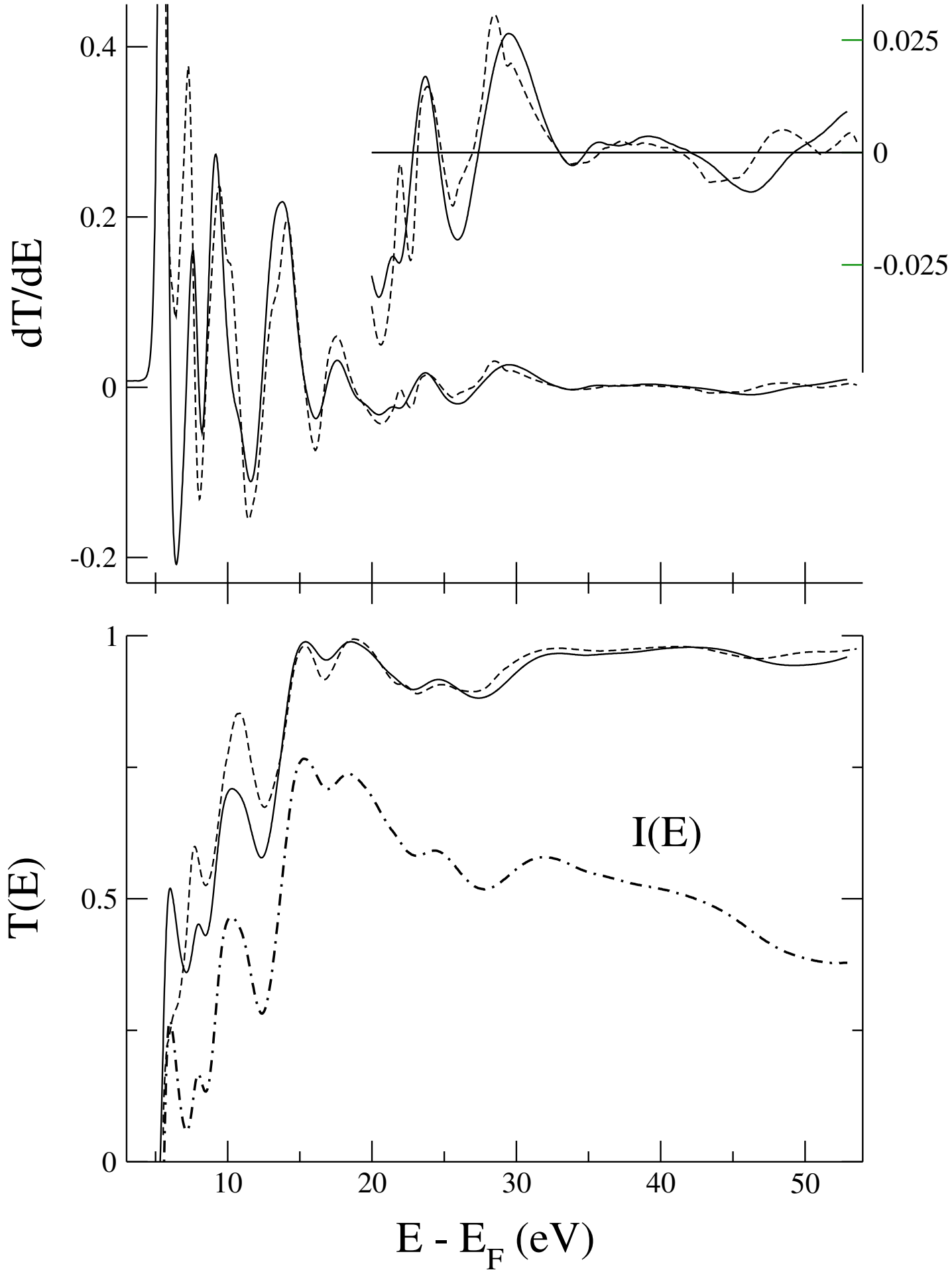
0.4
0.2
0
-0.2
dT/dE
0.025
0
-0.025
1
0.5
0
T(E)
I(E)
10
20
30
40
50
E - E_F (eV)

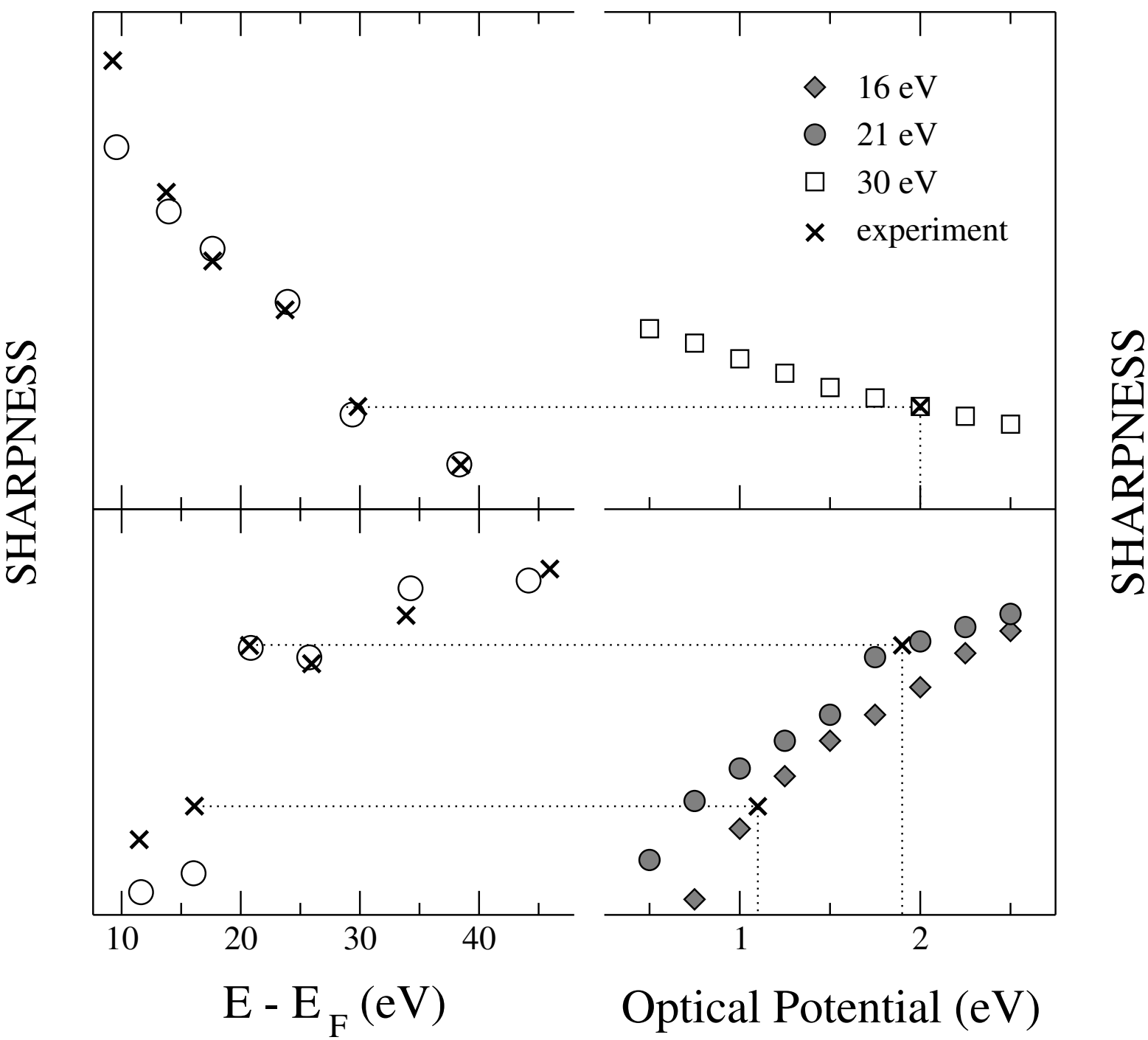
SHARPNESS
SHARPNESS
16 eV
21 eV
30 eV
experiment
10
20
30
40
1
2
E - E F (eV)
Optical Potential (eV)

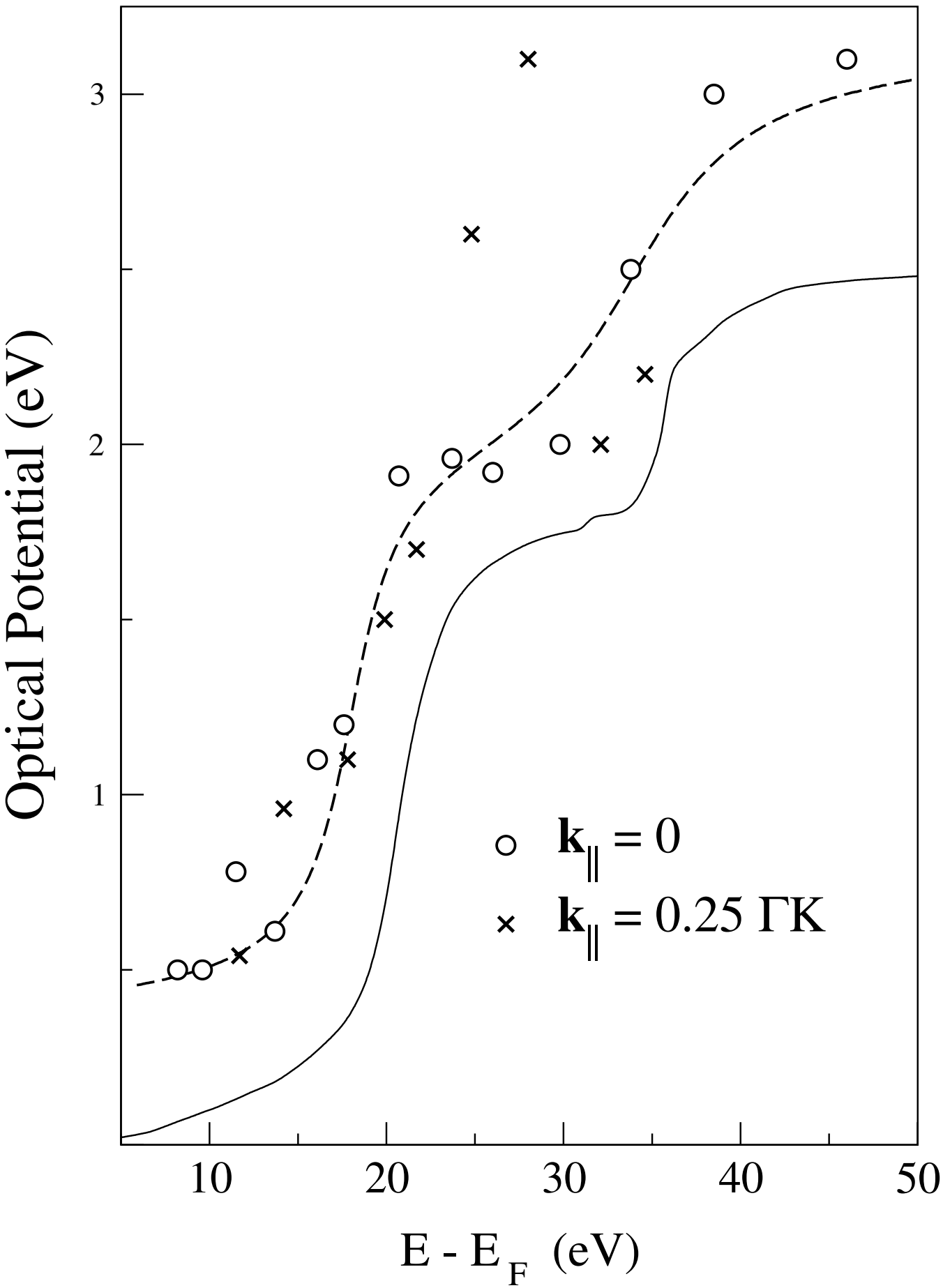
Optical Potential (eV)
3
2
1
10
20
30
40
50
E - E_F (eV)
k_∥ = 0
k_∥ = 0.25 ΓK

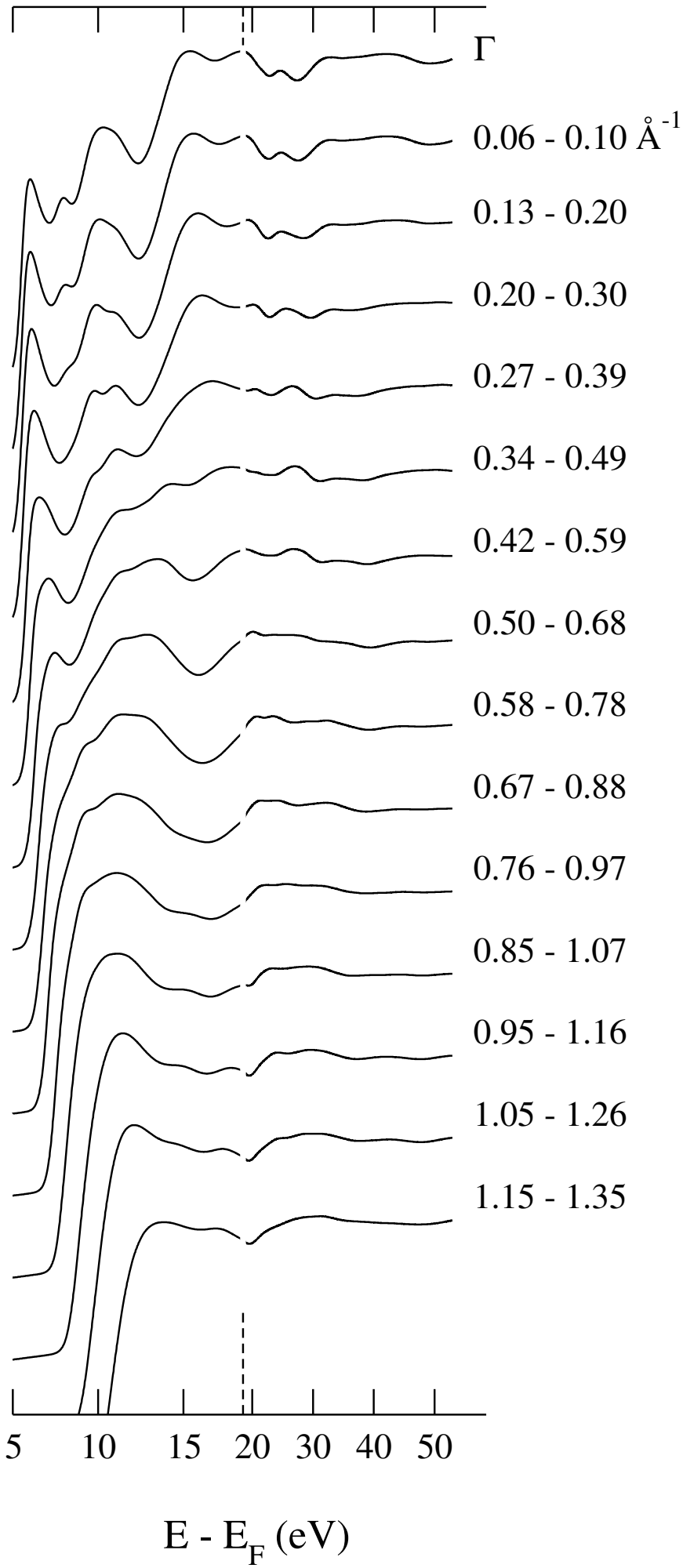
Γ
0.06 - 0.10 Å-1
0.13 - 0.20
0.20 - 0.30
0.27 - 0.39
0.34 - 0.49
0.42 - 0.59
0.50 - 0.68
0.58 - 0.78
0.67 - 0.88
0.76 - 0.97
0.85 - 1.07
0.95 - 1.16
1.05 - 1.26
1.15 - 1.35
5
10
15
20
30
40
50
E - EF (eV)

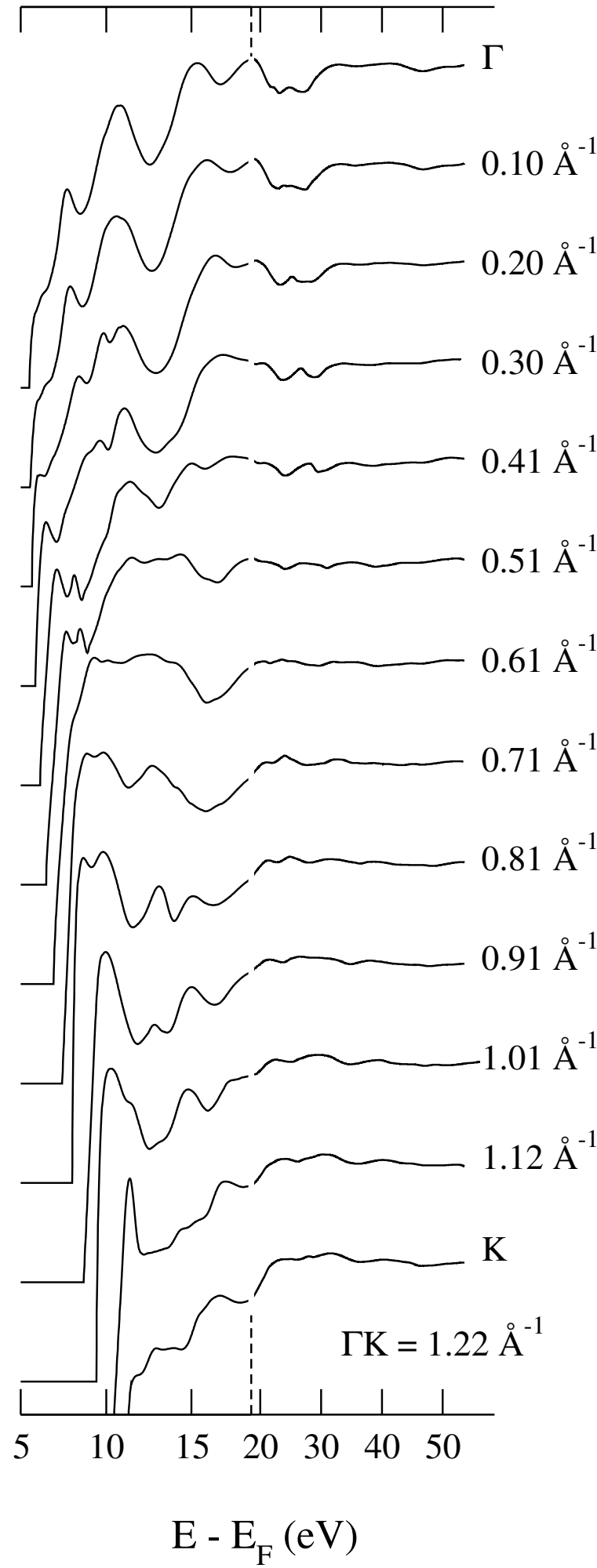
Γ
0.10 Å-1
0.20 Å-1
0.30 Å-1
0.41 Å-1
0.51 Å-1
0.61 Å-1
0.71 Å-1
0.81 Å-1
0.91 Å-1
1.01 Å-1
1.12 Å-1
K
ΓK = 1.22 Å-1
5
10
15
20
30
40
50
E - EF (eV)

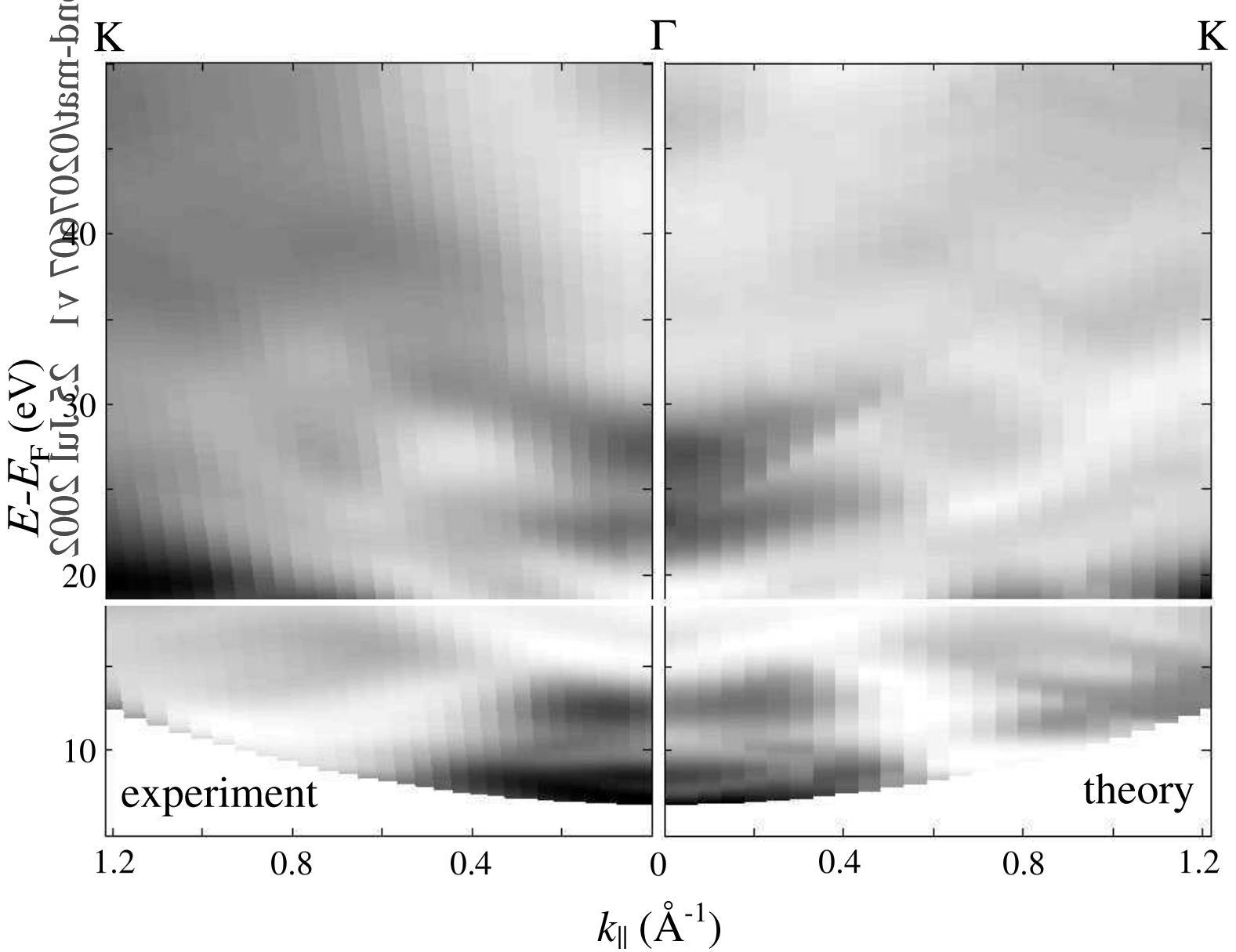
K
Γ
K
40
30
20
10
$E$-$E_F$ (eV)
experiment
theory
1.2
0.8
0.4
0
0.4
0.8
1.2
$k_{\parallel}$ (Å$^{-1}$)

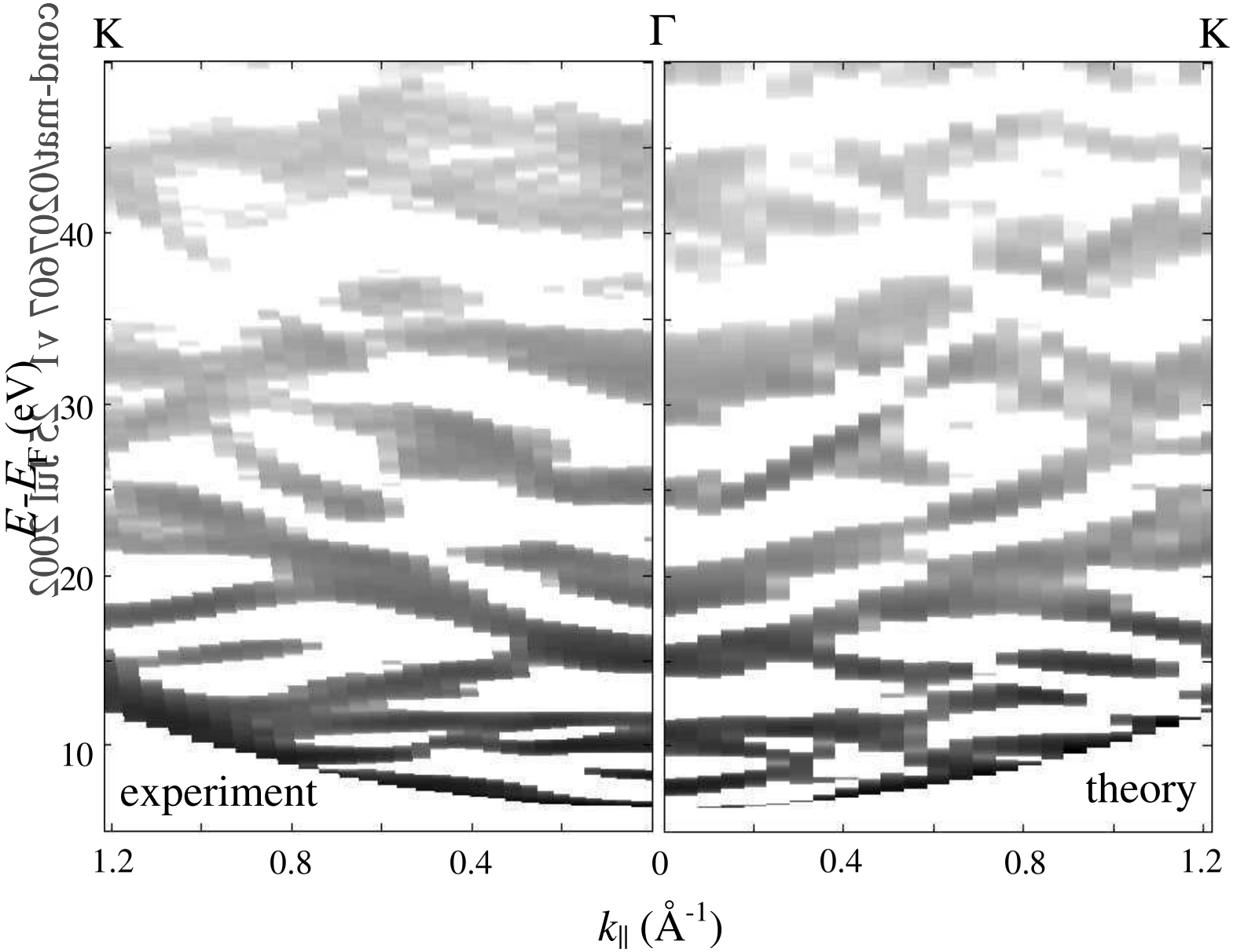
K
Γ
K
experiment
theory
$E-E_F$ (eV)
10
20
30
40
1.2
0.8
0.4
0
0.4
0.8
1.2
$k_{\parallel}$ (Å$^{-1}$)

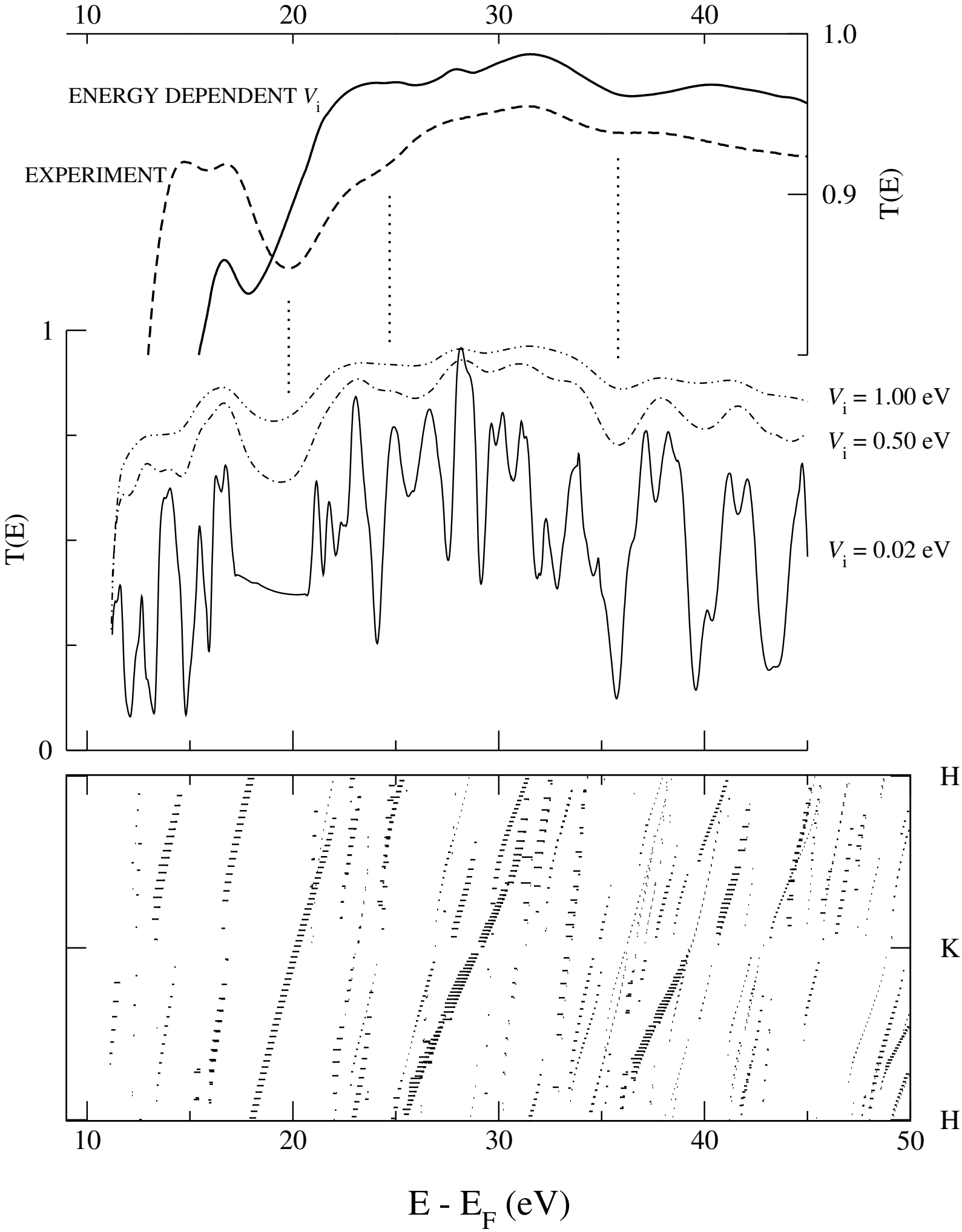
10
20
30
40
1.0
ENERGY DEPENDENT $V_i$
EXPERIMENT
0.9
T(E)
1
$V_i$ = 1.00 eV
$V_i$ = 0.50 eV
$V_i$ = 0.02 eV
T(E)
0
H
K
H
10
20
30
40
50
E - $E_F$ (eV)

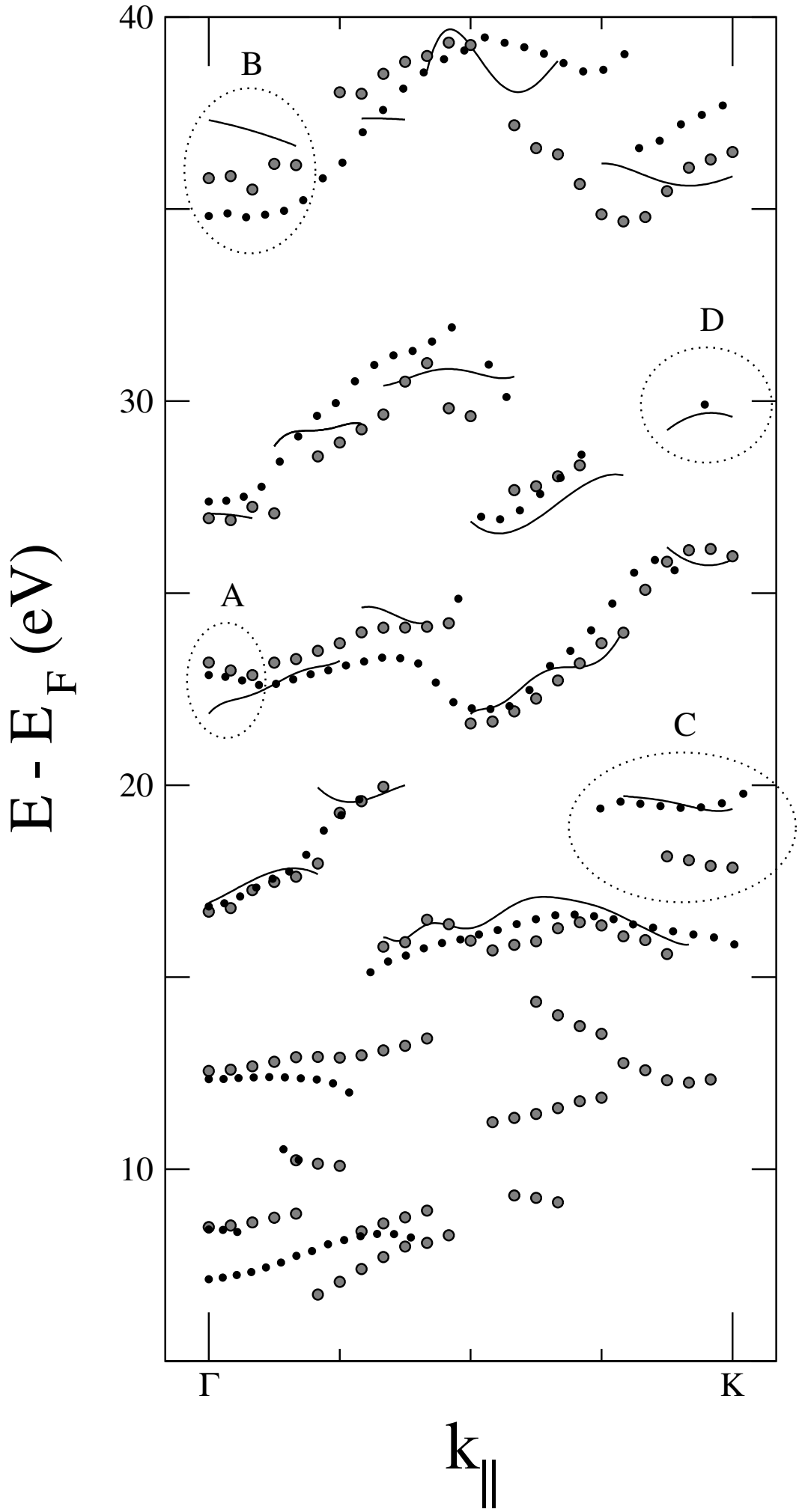
40
30
20
10
B
D
A
C
E - E_F (eV)
Γ
K
k_||

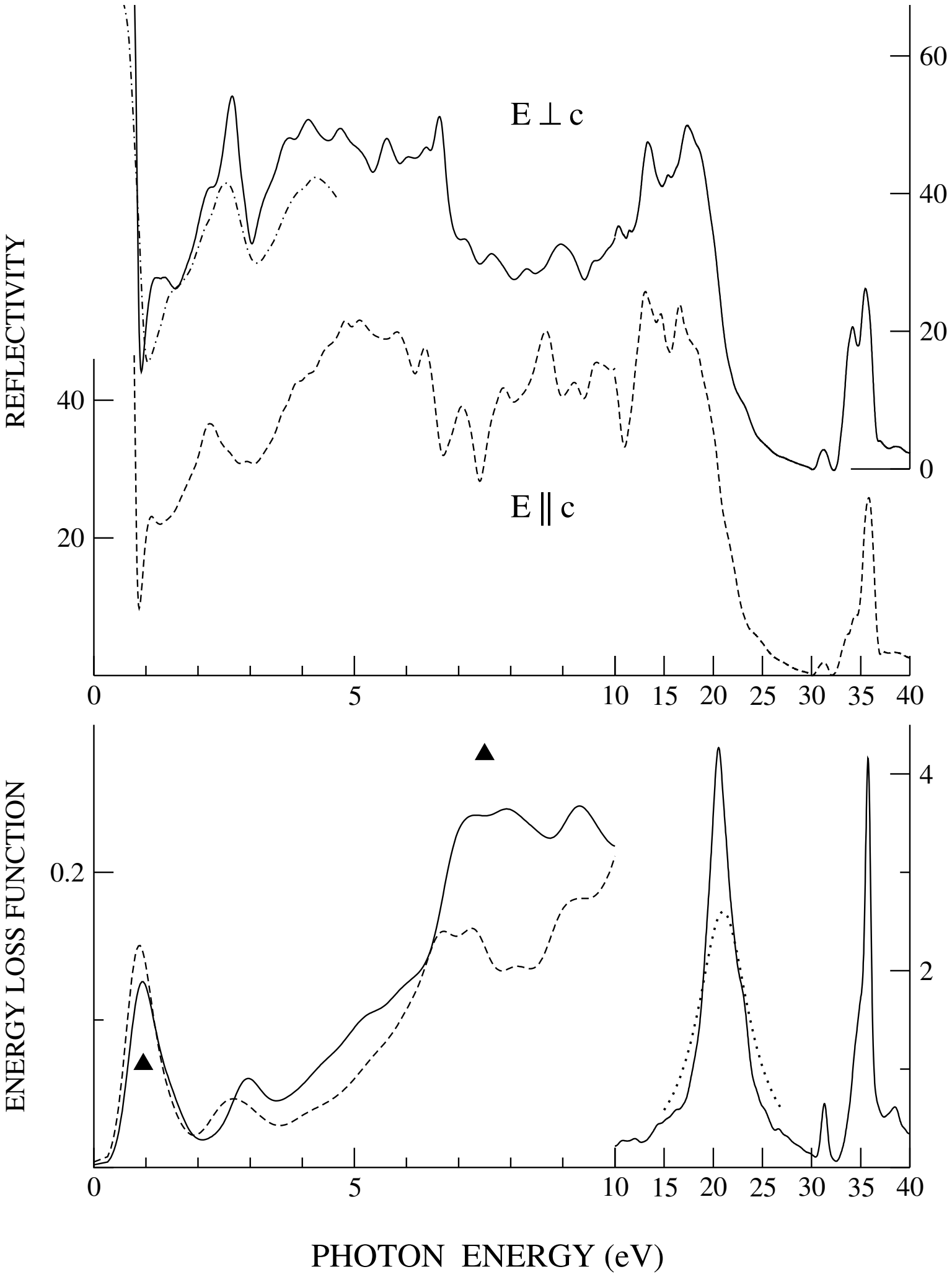
REFLECTIVITY
E ⊥ c
E ∥ c
60
40
20
0
40
20
0
5
10
15
20
25
30
35
40
ENERGY LOSS FUNCTION
0.2
4
2
PHOTON ENERGY (eV)